Brain MR image segmentation using multiphase active contours based on local and global fitter images.

AKRAM, F., SINGH, V.K., SARKER, M.M.K., GARCIA, M.A. and PUIG, D.

2018

May 2018

Brain MR Image Segmentation Using Multiphase Active Contours Based on Local and Global Fitted Images

Farhan AKRAM [a,1], Vivek Kumar SINGH [b], Md. Mostafa Kamal SARKER [b], Miguel Angel GARCIA [c], and Domenec PUIG [b]

[a] *Imaging Informatics Division, Bioinformatics Institute, 30 Biopolis Street, # 07-01, Matrix, 138671, Singapore.*

[b] *Department of Computer Engineering and Mathematics, Rovira i Virgili University, Tarragona 43003, Spain.*

[c] *Department of Electronic and Communications Technology, Autonomous University of Madrid, Madrid 28049, Spain.*

Abstract. The study of white matter (WM), grey matter (GM) and cerebrospinal fluid (CSF) regions in the brain magnetic resonance (MR) images can be useful for determining different brain disorders, assisting brain surgery, post-surgical analysis, saliency detection and for studying regions of interest. In this paper, a novel hybrid region-based multiphase (four-phase) active contours method is proposed to partition a brain MR image into three distinct regions i.e., GM, WM and CSF. The proposed energy functional is formulated by combining local and global fitted images in a multiplicative fashion. Both fitted images are defined by integrating two-phase global and local intensity from Chan-Vese (CV) and local binary fitted (LBF) models, respectively. In this paper, a post processing (pixel correction) method is also devised which improves the accuracy of the segmented WM, GM and CSF regions in a brain MR image. Different thresholds are decided based on averages of all three regions. According to the computed thresholds, a binary value (0 or 1) is then assigned to each pixel. Experimental results using both two-dimensional (2D) and three-dimensional (3D) brain MR images show that the proposed method outperforms the state-of-the-art both qualitatively and quantitatively.

Keywords. Active contours, multiphase, local and global fitted images, brain segmentation, pixel correction, thresholding.

1. Introduction

Brain MR imaging is a widely used imaging technology to study the brain anatomy and function. Segmentation of brain MR images into different disjoint regions: grey matter (GM), white matter (WM) and cerebrospinal fluid (CSF) can help physicians and doctors to carefully analyse head injuries, stroke, brain tumours and other brain diseases [1]. Aphasia in stroke patients may result from both WM and GM damage. Numerous

[1] Corresponding Author: Farhan Akram (farhana@bii.a-star.edu.sg)

speech therapies can help to treat such patients. However, it is very import to carefully analyse the change after each therapy session to decide if this therapy is effective or not. Therefore, a proper visual analysis of WM and GM region is critical for such cases [2].

Due to the geometric complexity of the human brain cortex, manual slice-by-slice segmentation is cumbersome and time consuming. Numerous methods have been devised to segment the brain into different non-overlapping regions [3]. In particular, the active contour method introduced in [4] is widely-used for medical image segmentation. In this method, a curve evolves towards the boundaries of the objects of interest under a certain force field by minimizing the curve's intrinsic energy.

A traditional region-based active contour method [5] is defined under the assumption that the target image is homogeneous. Therefore, it cannot properly segment images with intensity inhomogeneous regions. A region-based active contour method was proposed in the context of intensity inhomogeneous image segmentation [6]. It computes the image intensity mean over a local neighbourhood by using a Gaussian kernel.

Alternatively, a region-based active contour method for brain MR image segmentation was proposed in [7]. That method applies a locally-computed active contour method based on a signed pressure force (SPF) function in order to segment the brain into WM and GM regions. Since it is a two-phase active contour method, it can only segment the input images into two disjoint regions.

A multiphase level set framework (MLSF) using n level sets was proposed to segment a given image into 2^n phases (regions) [8]. It was developed under the assumption that the input image must have homogeneous intensity regions. Therefore, it does not properly work on images that contain inhomogeneous regions.

A variational level set approach for bias correction and segmentation (VLSBCS) of images corrupted with intensity inhomogeneities was proposed by Li et al. in [9]. The computed bias field is intrinsically ensured to be smooth by the data term in the variational formulation, without any additional effect to maintain the smoothness of the bias field. In this work, the two-phase model is also extended to a four-phase approach.

A local statistical active contour model (LSACM) for image segmentation in the presence of intensity inhomogeneity was proposed by Zhang et al. in [10]. In this method, inhomogeneous objects are modelled as Gaussian distributions of different means and variances. In this work, four-phase energy functional is also formulated along with a two-phase model. Therefore, it is suitable to segment brain MR images into the desired regions of interest i.e., WM, GM and CSF.

A hybrid region-based active contours driven by local and global fitted image models (LGFIM) was proposed in the context of intensity inhomogeneity [11]. Local and global intensity information were used to both correct and segment the inhomogeneous regions. Two SPF functions i.e., local and global were also devised to stabilize the gradient descent solution.

In this paper, a four-phase hybrid region-based active contour method is proposed to segment brain MR images into three regions of interests i.e., WM, GM and CSF. There are three main contributions of this work. First, a hybrid region-based multiphase active contour model is proposed by integrating local and global fitted images in a multiplicative manner. The proposed method combines two different two-phase fitted images to formulate a four-phase model, which has not been exploited before. Second, a post-processing (pixel correction) method is also devised to increase the segmentation accuracy of the regions of interest (WM, GM and CSF regions). Local active contour methods

are very sensitive to the initial position of the contour. Lastly, the proposed method uses fitted images based on both local and global intensity means, thus not being sensitive to the initial position of the contour.

2. Proposed method

A local image fitting energy functional is proposed by [12] in which the difference between the fitted image and the original image is minimized. In this paper, a novel multiphase (four-phase) image segmentation method is proposed to partition a brain MR image into three distinct regions using an image fitting energy functional. A four-phase active contours partition an image into four regions. However, the fourth region is discarded, since it contains unnecessary background information. The proposed four-phase fitted image (FFI) energy functional E_{FFI} is based on the product of two different two-phase fitted image differences to minimize the error, which is defined as follows:

$$E_{FFI} = E_{prop}(\Phi) + \mu \int_{\Omega} |\nabla H_{\varepsilon}(\phi_i)| dx + \nu \int_{\Omega} H_{\varepsilon}(\phi_i) dx, \tag{1}$$

where Φ is the function which represents two level sets (ϕ_1, ϕ_2), ϕ_i is an i^{th} level set curve and $i = 1, 2$. $\mu \geq 0$, $\nu \geq 0$ are fixed parameters. E_{prop} is the proposed four-phase energy functional. In (1), second and third terms are called length and area terms, respectively. The length term regularizes the curve and the area term smoothes the object to speed up the curve evolution.

Let $I : \Omega \rightarrow \mathbf{R}^2$ be the input image, $I_{GFI}(x)$ the global fitted image for the level set ϕ_1 and $I_{LFI}(x)$ the local fitted image for the level set ϕ_2. An energy functional for the proposed four-phase fitted image segmentation model E_{prop} can then be defined as:

$$E_{prop}(\Phi) = \frac{1}{2} \int_{\Omega} \big(I(x) - I_{GFI}(x)\big)\big(I(x) - I_{LFI}(x)\big) dx, \qquad x \in \Omega \tag{2}$$

where $I_{GFI}(x)$ and $I_{LFI}(x)$ are two-phase global and local fitted images for ϕ_1 and ϕ_2, respectively, which are defined as:

$$I_{GFI}(x) = m_1 M_1(\phi_1(x)) + m_2 M_2(\phi_1(x)), \tag{3}$$

$$I_{LFI}(x) = f_1 M_1(\phi_2(x)) + f_2 M_2(\phi_2(x)), \tag{4}$$

where $M_1(\phi_1) = H_{\varepsilon}(\phi_1)$, $M_2(\phi_1) = 1 - H_{\varepsilon}(\phi_1)$, $M_1(\phi_2) = H_{\varepsilon}(\phi_2)$ and $M_2(\phi_2) = 1 - H_{\varepsilon}(\phi_2)$ are characteristic terms defined for both level sets (ϕ_1 and ϕ_2) and $H_{\varepsilon}(\phi)$ is the regularized version of the Heaviside function as defined:

$$H_\varepsilon(\phi) = \frac{1}{2} + \frac{1}{\pi} arctan\Big(\frac{\phi}{\varepsilon}\Big), \tag{5}$$

In (3) and (4), (m_1, m_2) and (f_1, f_2) are global and local intensity means for level sets ϕ_1 and ϕ_2, respectively, which are defined as below:

$$m_i = \frac{\int\limits_\Omega I(x) M_i(\phi) dx}{\int\limits_\Omega M_i(\phi) dx}, \tag{6}$$

$$f_i(x) = \frac{K_\sigma * \big[I(x) M_i(\phi)\big]}{K_\sigma * M_i(\phi)}, \tag{7}$$

By using the calculus of variations and the steepest gradient descent [13], E_{prop} in (2) is minimized with respect to ϕ_1 and ϕ_2, leading to the corresponding gradient descent flows:

$$\frac{\partial \phi_1}{\partial t} = \big(I(x) - I_{LFI}(x)\big)(m_1 - m_2)\delta_\varepsilon(\phi_1), \tag{8}$$

$$\frac{\partial \phi_2}{\partial t} = \big(I(x) - I_{GFI}(x)\big)(f_1 - f_2)\delta_\varepsilon(\phi_2), \tag{9}$$

where $\delta_\varepsilon(\phi)$ is the regularized Dirac function, which is defined as:

$$\delta_\varepsilon(\phi) = \frac{\varepsilon}{\pi(\phi^2 + \varepsilon^2)}, \tag{10}$$

By using calculus of variations and applying steepest gradient descent [13], E_{FFI} in (1) is minimized with respect to ϕ_1 and ϕ_2 are following gradient descent flows are obtained:

$$\frac{\partial \phi_1}{\partial t} = \left(\big(I(x) - I_{LFI}(x)\big)(m_1 - m_2) + \mu \,\mathrm{div}\left(\frac{\nabla \phi_1}{|\nabla \phi_1|}\right) - v\right)\delta_\varepsilon(\phi_1), \tag{11}$$

$$\frac{\partial \phi_2}{\partial t} = \left(\big(I(x) - I_{GFI}(x)\big)(f_1 - f_2) + \mu \,\mathrm{div}\left(\frac{\nabla \phi_2}{|\nabla \phi_2|}\right) - v\right)\delta_\varepsilon(\phi_2), \tag{12}$$

A signed distance function (SDF) defined below is used for the initialization of the level set functions:

$$\phi_i(x,t=0) = \begin{cases} -\rho, & x \in \Omega_i - \partial\Omega_i \\ 0, & x \in \partial\Omega_i \\ \rho, & x \in \Omega - \Omega_i \end{cases} \tag{13}$$

where $\rho > 0$ is a constant ($\rho = 1$ in this work). In (13), $t = 0$ and $i = 1,2$ define the initial conditions of both level set functions. Ω_i is the inner region of the initial level set ϕ_i, Ω is the image domain and $\partial\Omega_i$ is the boundary of level set ϕ_i.

After evolving the level set functions using (11) and (12), they are regularized by using $\phi_i^k = G_\chi * \phi_i^k$, where $i = 1,2$ represents the number of level sets and k is the iteration number during the curve evolution. The regularization mentioned above not only regularizes the level set functions, but also eliminates the need for re-initialization, which is computationally very expensive. Here, χ is the standard deviation of the Gaussian kernel used in the regularization process.

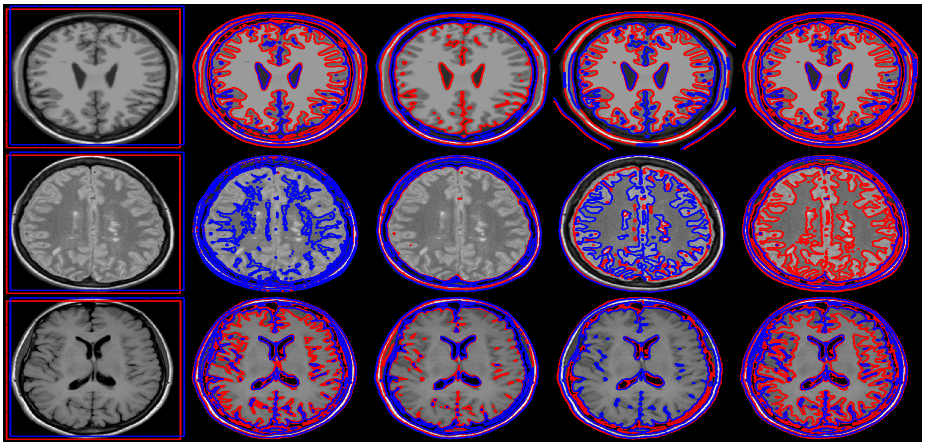

(a) (b) (c) (d) (e)

Figure 1. Four-phase segmentation comparison using a 2D brain MR image. (a) Initial contour, (b) MLSF, (c) VLSBCS, (d) LSACM, and (e) Proposed method.

Figure 1 shows the final four-phase segmentation result using the proposed and state-of-the-art methods. The proposed method segmented regions with more details, hence yielding better segmentation results.

3. Pixel correction

In this section, a thresholding-based post processing (pixel correction) method is proposed to improve the accuracy of the segmented WM, GM and CSF regions in a brain MR image. The segmentation results obtained from the proposed four-phase active contours are modified according to a pixel correction algorithm based on simple thresholding. The WM, GM and CSF binary regions computed in the previous stage are intersected with the input grey-level image to compute the intensity average of their non-zero pixels. These averages are then used to define a set of thresholds. If N is the number of

rows and columns ($N = 250$ in this work), the intensity means corresponding to the three regions of interest are respectively defined as:

$$\overline{WM} = \frac{\sum_{x=1}^{N}\sum_{y=1}^{N} I(x,y)WM(x,y)}{\sum_{x=1}^{N}\sum_{y=1}^{N} WM(x,y)}, \quad I(x,y) \neq 0 \tag{14}$$

$$\overline{GM} = \frac{\sum_{x=1}^{N}\sum_{y=1}^{N} I(x,y)GM(x,y)}{\sum_{x=1}^{N}\sum_{y=1}^{N} GM(x,y)}, \quad I(x,y) \neq 0 \tag{15}$$

$$\overline{CSF} = \frac{\sum_{x=1}^{N}\sum_{y=1}^{N} I(x,y)CSF(x,y)}{\sum_{x=1}^{N}\sum_{y=1}^{N} CSF(x,y)}, \quad I(x,y) \neq 0 \tag{16}$$

Different thresholds are decided by using the computed averages $\overline{WM}$, $\overline{GM}$ and $\overline{CSF}$ to construct new binary images for the WM, GM and CSF regions. Based on the decided bounds of the threshold, each pixel is assigned a binary value (0 or 1). The binary images corresponding to the regions of interest are finally defined as:

$$WM(x,y) = \begin{cases} 1, & \frac{\overline{WM}}{2} + 128 > I(x,y) \geq \frac{\overline{WM}+\overline{GM}}{2} \\ 0, & \text{Otherwise} \end{cases} \tag{17}$$

$$GM(x,y) = \begin{cases} 1, & \frac{\overline{WM}+\overline{GM}}{2} > I(x,y) \geq \frac{\overline{GM}+\overline{CSF}}{2} \\ 0, & \text{Otherwise} \end{cases} \tag{18}$$

$$CSF(x,y) = \begin{cases} 1, & \frac{\overline{GM}+\overline{CSF}}{2} > I(x,y) \geq \frac{\overline{CSF}}{2} \\ 0, & \text{Otherwise} \end{cases} \tag{19}$$

4. Quantitative analysis and results

In this section, 2D and 3D segmentation results of the proposed method are shown and compared with the state-of-the-art multiphase active contour methods. The Jaccard index (JI) [14], the Dice similarity coefficient (DSC) [15] and the Matthew's correlation coefficient (MCC) [16] are similarity metrics frequently used in set comparison. In this section, we used these similarity metrics for the quantitative analysis for both 2D and 3D segmentation analysis.

Table 1. Segmentation accuracy of the WM, GM and CSF regions with the tested methods using 2D slices.

Regions	Methods	JI	DSC	MCC
WM	MLSF	**92.52 ± 0.92**	**95.80± 0.67**	**95.21± 0.65**
	VLSBCS	84.88± 1.72	90.69± 1.23	89.84± 1.21
	LSACM	83.62 ± 1.30	90.46 ± 0.89	89.03 ± 0.95
	Proposed	91.97 ± 0.45	95.76 ± 0.25	95.06 ± 0.26
GM	MLSF	85.84 ± 1.96	90.34± 1.97	89.08± 1.94
	VLSBCS	73.22± 2.19	82.10 ± 1.95	79.21± 2
	LSACM	75.43 ± 1.43	84.99 ± 1.26	82.33 ± 1.40
	Proposed	**90.50 ± 0.23**	**95.00 ± 0.13**	**93.67 ± 0.16**
CSF	MLSF	64.71 ± 0.93	78.16 ± 0.74	78.97 ± 0.68
	VLSBCS	56.73± 0.81	72.05 ± 0.67	71.15 ± 0.59
	LSACM	59.66 ± 1.75	72.86 ± 1.74	72.54 ± 1.55
	Proposed	**82.69± 0.48**	**90.45± 0.30**	**89.82± 0.32**

Table 2. Segmentation accuracy of the WM, GM and CSF regions with the tested methods using 2D slices after applying pixel correction.

Regions	Methods	JI	DSC	MCC
WM	MLSF	94.14 ± 0.85	96.71 ± 0.63	96.21 ± 0.61
	VLSBCS	92.22 ± 1.01	95.58 ± 0.72	95.03 ± 0.69
	LSACM	94.32 ± 0.74	96.88 ± 0.52	96.38 ± 0.52
	Proposed	**94.59 ± 0.14**	**97.22 ± 0.07**	**96.64 ± 0.08**
GM	MLSF	91.71 ± 1.20	94.97 ± 1.14	94.20 ± 1.06
	VLSBCS	89.43 ± 1.26	93.73 ± 1.05	92.85 ± 0.96
	LSACM	88.71 ± 1.39	93.07 ± 1.30	92.18 ± 1.18
	Proposed	**93.41 ± 0.09**	**96.59 ± 0.05**	**95.69 ± 0.06**
CSF	MLSF	81.52 ± 0.38	89.77 ± 0.24	89.60 ± 0.22
	VLSBCS	83.75 ± 0.30	91.13 ± 0.18	90.79 ± 0.17
	LSACM	83.66 ± 0.78	90.81 ± 0.71	90.48 ± 0.67
	Proposed	**84.71 ± 0.26**	**91.70 ± 0.15**	**91.38 ± 0.15**

4.1. Two dimensional image segmentation

4.1.1. Data and selection of parameters

In this section, 2D segmentation results are shown using the proposed method. Moreover, segmentation results of the WM, GM and CSF regions are compared with the state-of-the-art method quantitatively. The proposed method was implemented using MATLAB and run on a 3.4 GHz Intel Core-i7 with 16 GB of RAM, testing it on a real brain magnetic resonance (MR) images of 250×250 pixels with 256 grey levels (8bpp) [17]. The parameters used in all experiments in this section are: $\mu = 25$, $v = 175$, $\sigma = 3$, $\chi = 0.5$, $\varepsilon = 1$ and time step $\tau = 0.001$.

4.1.2. Results

For 2D experiments, 100 2D slices from 20 patients (brain anatomical models) are used i.e., 5 slices (slice number 150, 175, 200, 225 and 250) for each patient. Table 1 shows a segmentation accuracy comparison of the WM, GM and CSF regions among the evaluated methods using the similarity metrics before applying the pixel correction algorithm. Both the mean and standard deviation (mean error) of the evaluated metrics are considered for all three brain regions, i.e., WM, GM and CSF. For the WM region, the MLSF

method yields the highest values for all similarity metrics. For this region, the proposed method has a JI of 91.97%, DSC of 95.76% and MCC of 95.06%, which is 0.55%, 0.04% and 0.15% less than the respective values computed by the MLSF method. In turn, the proposed method yields the best results for all similarity metrics for both GM and CSF regions.

Table 2 shows a segmentation accuracy comparison of the WM, GM and CSF regions among the evaluated methods using the similarity metrics after applying the pixel correction algorithm. It shows that the proposed method yields the best values for all similarity metrics among the evaluated methods for all regions of the interest i.e., WM, GM and CSF regions.

4.2. Volumetric data segmentation using 3D brain models

4.2.1. Data and selection of parameters

In this section, segmentation results of the proposed method and the state-of-the-art are compared using 20 brain MR anatomical models [17]. In all images, the range of intensities is represented from 0 to 255 grey levels, while the size in voxels ($length \times width \times height$) is ($250 \times 250 \times 362$). The parameters of the proposed method are the same as those given in section 4.1.

4.2.2. Results

Table 3 shows that after applying pixel correction, the proposed method improves the results of the similarity metrics (JI, DSC and MCC) by 9.42%, 5.51% and 5.8% for the WM region, 9.5%, 5.66% and 6.64% for the GM region and 7.37%, 4.88% and 5.26% for the CSF region, respectively.

Table 3. 3D segmentation accuracy of the WM, GM and CSF regions before and after pixel correction.

Regions	Similarity metrics	Proposed method without pixel correction	Proposed method with pixel correction
WM	JI	81.35 ± 1.07	$\mathbf{90.77 \pm 0.28}$
	DSC	89.65 ± 0.89	$\mathbf{95.16 \pm 0.23}$
	MCC	88.94 ± 0.85	$\mathbf{94.74 \pm 0.22}$
GM	JI	81.31 ± 1.37	$\mathbf{90.81 \pm 0.35}$
	DSC	89.51 ± 1.16	$\mathbf{95.17 \pm 0.30}$
	MCC	87.78 ± 1.11	$\mathbf{94.42 \pm 0.27}$
CSF	JI	77.09 ± 0.39	$\mathbf{84.46 \pm 0.26}$
	DSC	86.68 ± 0.32	$\mathbf{91.56 \pm 0.22}$
	MCC	85.99 ± 0.30	$\mathbf{91.25 \pm 0.21}$
CPU time (s)		$\mathbf{2.87} \times 10^3$	2.88×10^3

Figure 2 shows the segmented WM, GM and CSF regions of the brain MR volumetric data using different state-of-the art methods before and after applying the pixel correction algorithm. WM_1, GM_2 and CSF_1 refer to the segmented regions before applying pixel correction. In turn, WM_2, GM_2 and CSF_2 are the segmented regions obtained after applying pixel correction. Visually, it can be seen that the pixel correction algorithm significantly improves the segmentation results of all methods. Therefore, the proposed pixel correction method can be used in computer aided diagnosis (CAD) systems of brain MR images to improve the end results.

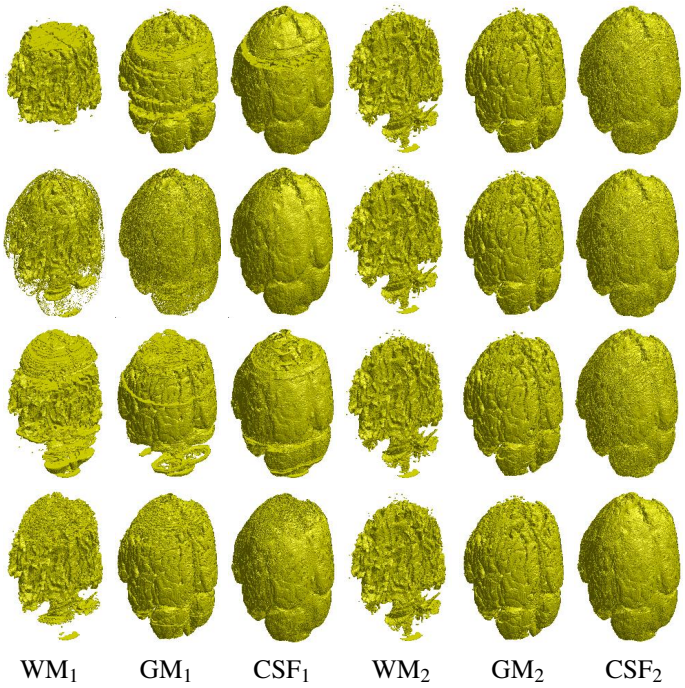

Figure 2. Comparison of volumetric segmentation results of WM, GM and CSF regions. Segmentation results using MLSF (first row), VLSBCS (second row), LSACM (third row) and proposed method (last row), respectively.

5. Conclusions and future work

Segmenting brain MR image into three different disjoint regions i.e., WM, GM and CSF is beneficial from various medical and psychological perspectives. In this paper, a four-phase active contour method is proposed to segment brain MR images into the WM, GM and CSF regions. The idea is to formulate a squared difference for the four-phase model by multiplying two different two-phase differences from the different level sets, which helps to reduce the mathematical complexity of the model. Moreover, a post processing (pixel correction) method is used, which improves the accuracy of the segmented regions significantly. The results show that the developed pixel correction algorithm works properly for all state-of-the-art methods that have been evaluated. Therefore, it can be used to improve the segmentation results of the WM, GM and CSF regions from all intensity-based methods. The proposed method yields better segmentation accuracy both qualitatively and quantitatively than the state-of-the-art methods for both 2D and 3D (volumetric data) images.

References

[1] Y. Zhang, B.J. Matuszewski, L.-K. Shark and C.J. Moore, A novel medical image segmentation method using dynamic programming, in: *International Conference on*

Medical Information Visualisation-BioMedical Visualisation, MediVis'07., IEEE, 2007, pp. 69–74.

[2] Y.-O. Li, F.G. Yang, C.T. Nguyen, S.R. Cooper, S.C. LaHue, S. Venugopal and P. Mukherjee, Independent component analysis of DTI reveals multivariate microstructural correlations of white matter in the human brain, *Human Brain Mapping* **33**(6) (2012), 1431–1451.

[3] A. Elnakib, G. Gimelfarb, J.S. Suri and A. El-Baz, Medical image segmentation: A brief survey, in: *Multi Modality State-of-the-Art Medical Image Segmentation and Registration Methodologies*, Springer, 2011, pp. 1–39.

[4] M. Kass, A. Witkin and D. Terzopoulos, Snakes: Active contour models, *International Journal of Computer Vision* **1**(4) (1988), 321–331.

[5] T.F. Chan and L.A. Vese, Active contours without edges, *IEEE Transactions on Image processing* **10**(2) (2001), 266–277.

[6] C. Li, C.-Y. Kao, J.C. Gore and Z. Ding, Minimization of region-scalable fitting energy for image segmentation, *IEEE Transactions on Image Processing* **17**(10) (2008), 1940–1949.

[7] F. Akram, J.H. Kim, H.U. Lim and K.N. Choi, Segmentation of Intensity Inhomogeneous Brain MR Images Using Active Contours, *Computational and Mathematical Methods in Medicine* **2014** (2014), 194614–119461414.

[8] L.A. Vese and T.F. Chan, A multiphase level set framework for image segmentation using the Mumford and Shah model, *International Journal of Computer Vision* **50**(3) (2002), 271–293.

[9] C. Li, R. Huang, Z. Ding, J.C. Gatenby, D.N. Metaxas and J.C. Gore, A level set method for image segmentation in the presence of intensity inhomogeneities with application to MRI, *IEEE Transactions on Image Processing* **20**(7) (2011), 2007–2016.

[10] K. Zhang, L. Zhang, K.-M. Lam and D. Zhang, A level set approach to image segmentation with intensity inhomogeneity, *IEEE Transactions on Cybernetics* **46**(2) (2016), 546–557.

[11] F. Akram, M.A. Garcia and D. Puig, Active contours driven by local and global fitted image models for image segmentation robust to intensity inhomogeneity, *PLOS ONE* **12**(4) (2017), 1–34.

[12] K. Zhang, H. Song and L. Zhang, Active contours driven by local image fitting energy, *Pattern Recognition* **43**(4) (2010), 1199–1206.

[13] G. Aubert and P. Kornprobst, *Mathematical Problems in Image Processing: Partial Differential Equations and the Calculus of Variations*, 2nd edn, Springer, New York, 2006.

[14] P. Jaccard, The distribution of the flora in the alphine zone, *The New Phytologist* **XI**(2) (1912), 37–50.

[15] L.R.. Dice, Measures of the Amount of Ecologic Association Between Species, *Ecology* **26**(3) (1945), 297–302.

[16] B.W. Matthews, Comparison of the predicted and observed secondary structure of T4 phage lysozyme, *BBA - Protein Structure* **405**(2) (1975), 442–451.

[17] B. Aubert-Broche, *Brain web: Anatomical models of 20 normal brains*, 2006, `http://brainweb.bic.mni.mcgill.ca/brainweb/anatomic_normal_20.html` [Accessed: April 24, 2015].